Optimising crystallisation during rapid prototyping of Fe3O4-PA6 polymer nanocomposite component.

GUPTA, R., NJUGUNA, J. and PANCHOLI, K.

2022

Journal of
Composites Science

MDPI

Article

Optimising Crystallisation during Rapid Prototyping of Fe_3O_4-PA6 Polymer Nanocomposite Component

Ranjeetkumar Gupta [1,2,3,*], James Njuguna [1] and Ketan Pancholi [1,*]

[1] School of Engineering, Robert Gordon University, Aberdeen AB10 7AQ, UK; j.njuguna@rgu.ac.uk
[2] Institute of Chemical Sciences, School of Engineering & Physical Sciences, Heriot-Watt University, Edinburgh EH14 4AS, UK
[3] Smart Systems Group, Institute of Sensors, Signals and Systems, School of Engineering & Physical Sciences, Heriot-Watt University, Edinburgh EH14 4AS, UK
* Correspondence: r.gupta@hw.ac.uk (R.G.); k.pancholi2@rgu.ac.uk (K.P.)

Abstract: Polymer components capable of self-healing can rapidly be manufactured by injecting the monomer (ε-caprolactam), activator and catalyst mixed with a small amount of magnetic nanoparticles into a steel mould. The anionic polymerisation of the monomer produces a polymer component capturing magnetic nanoparticles in a dispersed state. Any microcracks developed in this nanocomposite component can be healed by exposing it to an external alternating magnetic field. Due to the magnetocaloric effect, the nanoparticles locally melt the polymer in response to the magnetic field and fill the cracks, but the nanoparticles require establishing a network within the matrix of the polymer through effective dispersion for functional and uniform melting. The dispersed nanoparticles, however, affect the degree of crystallinity of the polymer depending on the radius of gyration of the polymer chain and the diameter of the magnetic nanoparticle agglomerates. The variation in the degree of crystallinity and crystallite size induced by nanoparticles can affect the melting temperature as well as its mechanical strength after testing for applications, such as stimuli-based self-healing. In the case of in situ synthesis of the polyamide-6 (PA6) magnetic nanocomposite (PMC), there is an opportunity to alter the degree of crystallinity and crystallite size by optimising the catalyst and activator concentration in the monomer. This optimisation method offers an opportunity to tune the crystallinity and, thus, the properties of PMC, which otherwise can be affected by the addition of nanoparticles. To study the effect of the concentration of the catalyst and activator on thermal properties, the degree of crystallinity and the crystallite size of the component (PMC), the ratio of activator and catalyst is varied during the anionic polymerisation of ε-caprolactam, but the concentration of Fe_3O_4 nanoparticles is kept constant at 1 wt%. Differential Scanning Calorimetry (DSC), Fourier-transform infrared spectroscopy (FTIR), XRD (X-ray diffraction) and Thermogravimetric analysis (TGA) were used to find the required concentration of the activator and catalyst for optimum properties. It was observed that the sample with 30% N-acetyl caprolactam (NACL) (with 50% EtMgBr) among all of the samples was most suitable to Rapid Prototype the PMC dog-bone sample with the desired degree of crystallinity and required formability.

Keywords: degree of crystallinity; polyamide-6; rapid prototyping; nanocomposite; self-healing

check for updates

Citation: Gupta, R.; Njuguna, J.; Pancholi, K. Optimising Crystallisation during Rapid Prototyping of Fe_3O_4-PA6 Polymer Nanocomposite Component. *J. Compos. Sci.* **2022**, *6*, 83. https://doi.org/10.3390/jcs6030083

Academic Editor: Francesco Tornabene

Received: 27 January 2022
Accepted: 1 March 2022
Published: 7 March 2022

Publisher's Note: MDPI stays neutral with regard to jurisdictional claims in published maps and institutional affiliations.

1. Introduction

Dispersing magnetic nanoparticles into the semi-crystalline thermoplastic PA6 (Polyamide 6) is useful for preparing a polymer nanocomposite (PMC) capable of self-healing a composite component by induced stimuli. The matrix of PA6 is versatile for engineering applications due to its ability to rapidly polymerise and provide good mouldability as well as mechanical properties [1–5]. PMCs with different functionalities or multifunctionalities can be produced using different types of nanoparticles (NPs) (Figure 1); however, the uniform dispersion of NPs is a precondition to achieve the required functionality. Previously, many nanoparticle dispersion techniques, such as melt blending,

solution blending, high-shear mixing and in situ polymerisation, have been used [3–8]. However, the in situ PMC manufacturing method is most favoured for preparing PA6 PMC, as it provides the ease of mixing the nanoparticles in a low-viscosity ε-caprolactam monomer before the activator/catalyst-mediated polymerisation [9] is carried out, ensuring effective dispersion. The incorporation of magnetic nanoparticles (MNPs), such as Fe_3O_4, using in situ methods has been proven to be useful in achieving melting through the magnetocaloric effect; however, its inclusion modifies the degree of crystallinity and resulting properties of the magnetic PA6 polymer [3]. Due to interface adhesion and MNPs dispersion, the degree of crystallinity and the crystalline structure within the polymer are affected [3,4], which, in turn, affects the multifunctional properties of the synthesised polymer magnetic PMC [1,10–12].

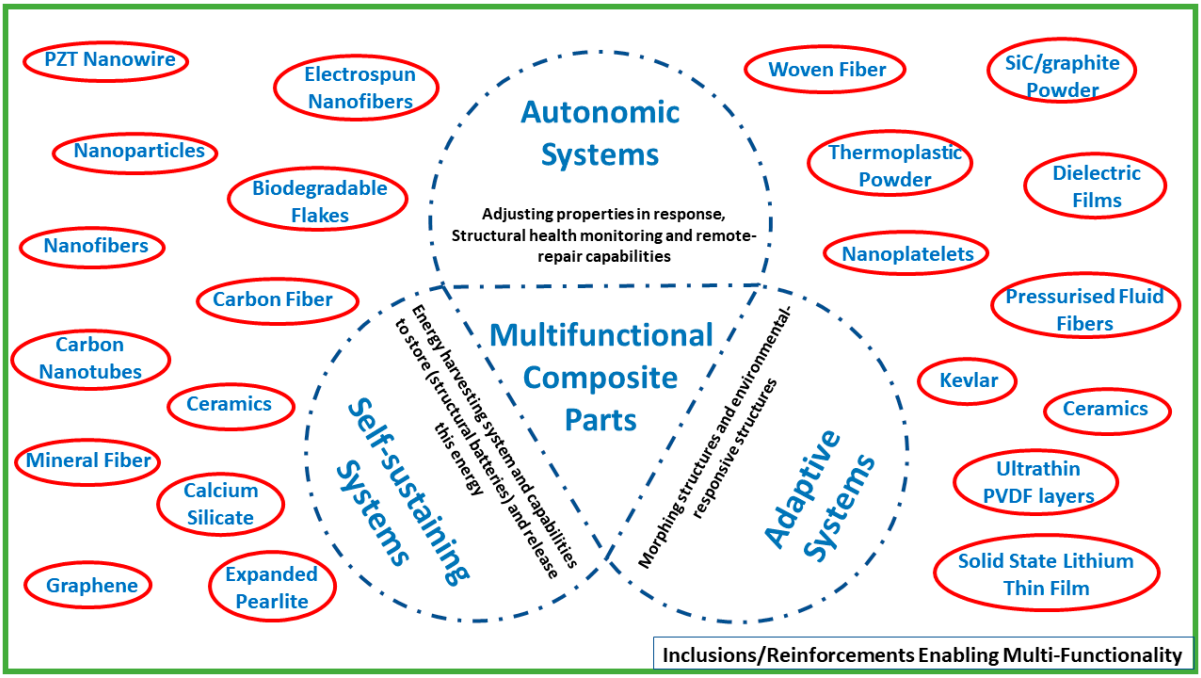

Figure 1. Various inclusions/reinforcements utilised for enhancing multifunctional features in composite materials.

In many instances, the required concentration of the nanoparticles and their size can unfavourably change the degree of crystallinity of the PMC, resulting in a hard and stiff polymer that cannot be formed into a flexible component. This often leads to the limited application of multifunctional PMCs, as such PMCs cannot be formed into a component [13]. Controlling the degree of crystallinity is a possible option to ensure the suitability of the PMC for further processing (e.g., injection moulding, film extrusion, etc.) and to reduce the challenge in its applicability for such applications [14]. Additionally, it is feasible to control the degree of crystallinity of the PMC by altering the concentration of the catalyst and activator for polymerisation. In order to offset the MNP-induced change in the degree of crystallinity of the polymer, the concentration of the catalyst and activator during PA6 polymerisation can be optimised.

Therefore, it is critical to investigate the effects on crystallinity and the resulting morphology under quiescent crystallisation due to the addition of different concentrations of the catalyst and the activator during anionic polymerisation [15]. The concentration of iron oxide nanoparticles is kept constant at 1 wt% when investigating the effect of the above parameters on the semi-crystalline morphologies, as it would dictate the macroscopic properties of the synthesised PMC [16,17].

Since the in situ polymerisation process depends on a suitable combination of catalyst and activator to bring about the polymerisation of the monomer, it is obvious that the rate of

polymerisation will affect the crystal growth and also the variable phase transformation [18]. This paper discusses the effect of the catalyst and the activator concentrations on the properties of polymerised PA6-PMC containing 1 wt% uncoated MNPs. The focus herein is to tune the degree of crystallinity of the prepared PA6-PMC for the optimum response in the rapid manufacturing process. The study is divided into three parts for studying the (i) catalyst variation, (ii) activator variation and (iii) both catalyst and activator variation simultaneously. Based on the comparison of the results of these variation studies, an optimum catalyst and activator proportion is proposed to be employed for the rapid prototyping method of composite part manufacturing.

2. Experimental Section

2.1. Materials

The ε-caprolactam (CL) (99% purity), 3.0 M ethyl magnesium bromide (EtMgBr–Grignard reagent) solution in diethyl ether, N-Acetyl Caprolactam (NACL) (99% purity) and Iron(III) oxide MNPs (<50 nm particle size), were purchased from Sigma–Aldrich Company Ltd. Dorset, UK, and used as received. The deionised water with 18 MO conductivity was used throughout the experiment.

2.2. Experimental Methods

Firstly, 30 g of CL was melted at 60 °C and MNPs were introduced into the melted monomer to prepare a 1 wt% iron oxide suspension. Subsequently, the iron oxide suspension was sonicated at 20 kHz for 30 min to ensure effective dispersion of the MNPs. Afterwards, the temperature was raised to 150 °C and EtMgBr was added in varying concentrations under an inert gas atmosphere. To complete the polymerisation, the required amount of NACL was added at 160 °C. The mixture was then left for polymerisation. Finally, the PMC samples were thoroughly washed with deionised water (18 MΩ cm) at 100 °C to remove any unreacted monomer, activator and catalyst. A total of three PMC samples for each catalyst/activator concentration were prepared for the study.

The reaction for the anionic polymerisation of CL is described by the following three equations:

i. Deprotonation of CL in presence of EtMgBr.

$$\text{EtMgBr} + \text{CL} \rightarrow \text{CLMgBr} + \text{Ethane (Catalyst formation Stage)}$$

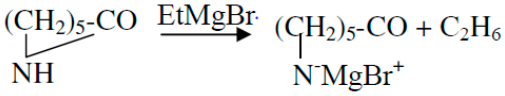

(1)

ii. Complex formation or activated initiation stage under the presence of NACL as an activator.

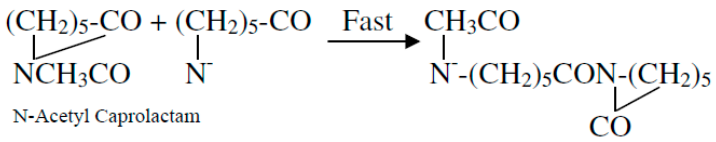

(2)

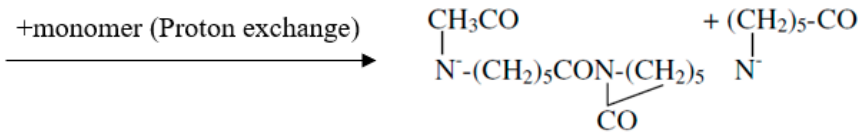

iii. Start of polymer chain propagation.

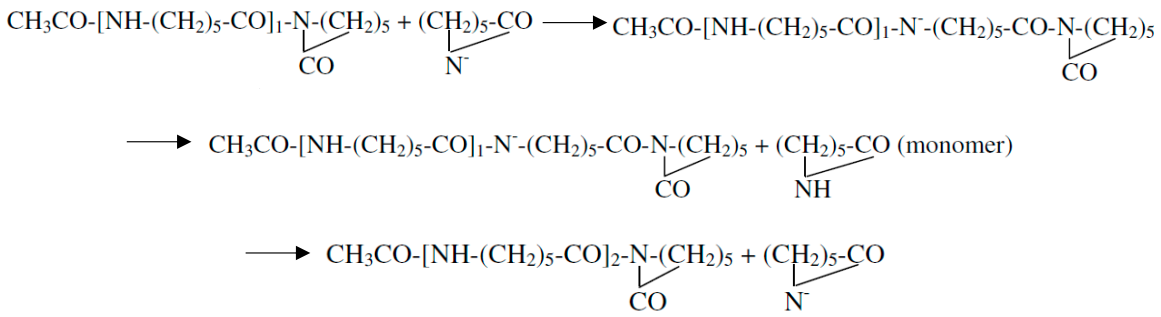

(3)

Sample Preparation

Adding nanoparticles to polymers changes the crystallinity and, therefore, changes the mechanical properties for better or worse. If PMC is produced using in situ polymerisation, there is an opportunity to modify the degree of crystallinity. To demonstrate the method to alter the crystallinity of the polymer in this work, the amount of nanoparticles added was kept constant to synthesise the anionic ring-opening polymerisation of the polyamide -6 (PA6) using three sets of parameters. The anionic ring-opening polymerisation of e-caprolactam was performed using Grignard reagent as a catalyst and N-acetyl caprolactam as an activator. In the first set of experiments, the activator concentration was kept constant and the catalyst concentration was varied, as shown in Table 1. The second set of experiments were run by keeping the catalyst concentration constant and varying the concentration of the activator. In the final set of experiments, both the activator and catalyst concentrations were varied to find out their effect on the thermal properties, degree of crystallinity and type of crystallites of the PMC. The variation in the concentrations of activator and catalyst for all three sets of experiments are shown in Table 1.

Table 1. Values of the concentrations of the catalyst (EtMgBr) and activator (NACL) used in all three sets of experiments.

At a Constant Activator Concentration, Values of Variable Catalyst (EtMgBr) Concentrations				
Sample	**Proportion**	**EtMgBr (mL)**	**NACL (mL)**	**Polymerisation Time (mins.)**
1	10%	0.0286	0.1600	1:40–2:05
2	30%	0.0858	0.1600	1:25–1:43
3	50%	0.1430	0.1600	1:10–1:34
4	70%	0.2002	0.1600	1:05–1:30
5	100%	0.2860	0.1600	1:00–1:25
At a Constant Catalyst Concentration, Values of Variable Activator (NACL) Concentrations				
Sample	**Proportion**	**EtMgBr (mL)**	**NACL (mL)**	**Polymerisation Time (mins.)**
1	10%	0.143	0.032	2:10–2:25
2	30%	0.143	0.096	1:50–2:05
3	50%	0.143	0.160	1:35–1:55
4	70%	0.143	0.224	1:15–1:30
5	100%	0.143	0.320	1:05–1:20

Table 1. *Cont.*

Values of Variable Activator (NACL) Concentrations and Variable Catalyst (EtMgBr) Concentrations				
Sample	**Proportion**	**EtMgBr (mL)**	**NACL (mL)**	**Polymerisation Time (mins.)**
1	10%	0.0286	0.0320	3:40–4:10
2	30%	0.0858	0.0960	3:00–3:35
3	50%	0.1430	0.1600	2:15–2:40
4	70%	0.2002	0.2240	1:30–1:45
5	100%	0.2860	0.3200	1:05–1:20

2.3. Material Characterisation

2.3.1. Differential Scanning Calorimetry (DSC)

DSC was performed by heating 9 mg of PMC at a rate of 10 °C/min under a nitrogen environment with a temperature range of 20 to 270 °C. The Heat/Cool/Heat standard cycle was selected on a TA Instruments DSC Q100 for accurately depicting the T_g and T_m. The running segment consisted of a ramp heating at 10 °C/min to 250 °C, then ramp cooling at 5 °C/min to −90 °C and finally ramp heating at 10 °C/min to 250 °C. The glass transition temperature (T_g) and melting temperature (T_m) were determined from the DSC traces obtained, where the first small endothermic peak represented the glass transition temperature, and the second larger endothermic peak represented the melting temperature of the PMC sample.

The monomer conversion in this study was measured by weighing the samples before and after the DSC run. Since all of the CL starts evaporating much before the T_m of PA6, and around the max DSC temperature, the sample is supposed to be CL free, the weight difference before and after the DSC gives the monomer conversion rate as per the following formula.

$$\text{Monomer Conversion Rate (\%)} = \frac{\text{Weight of Sample after DSC Run}}{\text{Weight of Sample before DSC Run}} \times 100 \quad (4)$$

2.3.2. Thermogravimetric Analysis (TGA)

TGA was performed on a sample mass of 7–12 mg using a TA Instruments TGA Q500. The heating rate was 10 °C/min and the 100% weight reduction mode was selected for the analysis. The measurements were conducted under an air atmosphere

2.3.3. Fourier Transform Infrared Spectroscopy (FTIR)

The Perkin–Elmer ATR–FTIR (Attenuated Total Reflection–Fourier Transmission Infrared Spectroscope) Spectrum Gx system containing a DGS–KBr sensor was used to identify the phases, bonds and structural changes that took place due to the polymerisation process and the addition of the iron oxide MNPs. PMC films of approximately 0.1 mm thickness were scanned 30 times between 525–4000 cm^{-1} at a resolution of 4 cm^{-1}. The gain was set to 2 and the optical velocity to 0.4747 m/s.

2.3.4. X-ray Diffraction (XRD)

A PANalytical X'Pert Pro MPD, powered by a Philips PW3040/60 X-ray (Cu-Kα, wavelength (λ) of 1.5418 Å) generator and fitted with an X'Celerator detector, was used to acquire the diffraction data. X-rays were generated from a Cu anode supplied with 40 kV and a current of 40 mA. The data were collected over a range of 0 to 60° (2θ) with a step size of 0.117° (2θ) and nominal time per step of 1099.82 using a scanning X'Celerator detector. Fixed anti-scatter and divergence slits of 0.38 mm were used together with a beam

mask of 10 mm to scan in a continuous mode. Phases were identified using the X'Pert-PRO accompanying software PANalytical High Score Plus in conjunction with the JCPDS card.

2.4. Composite Part Rapid Prototyping

To ensure proper mixture and synthesis of the PA6 composite part, the setup of two glass syringes connected with a manufactured 'Y' connector was used with the standard dog-bone mould already containing the CFRP prepreg, as shown in Figure 2.

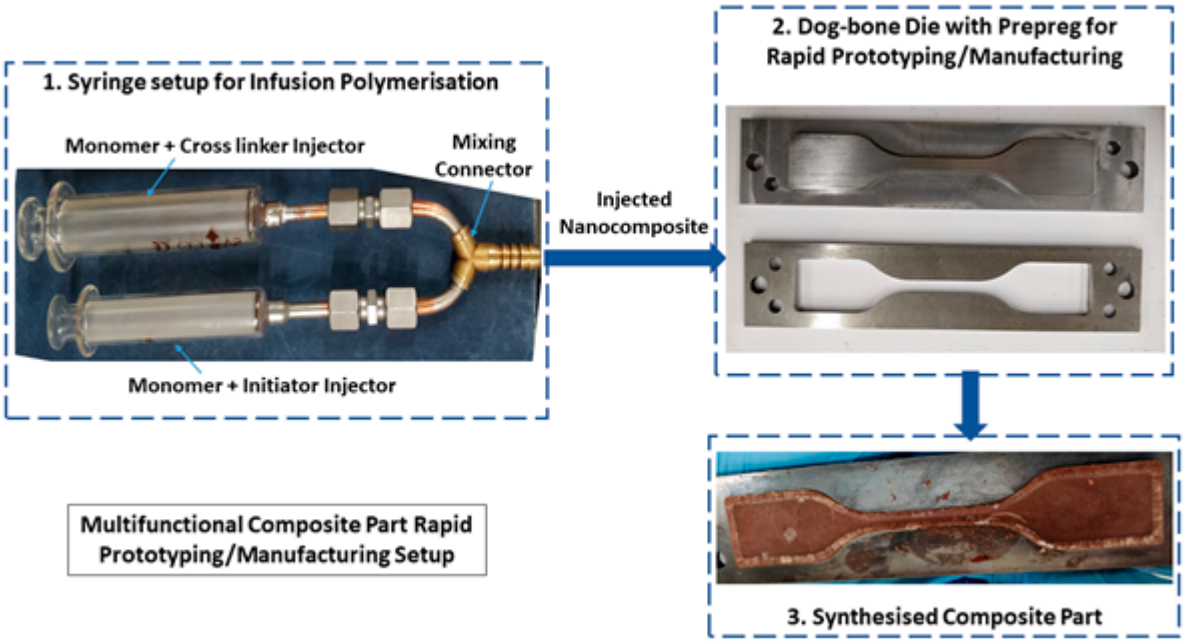

Figure 2. Individual polymer components prepared using a rapid prototyping/manufacturing setup, with the process sequence highlighted.

The various concentrations were tested and then the final optimised concentrations suitable for achieving the highest degree of crystallinity and lowest crystallite size was used to manufacture the dog-bone composite sample using this setup.

For manufacturing the PMC dog-bone sample, 30 g of monomer was taken and split into 20 g and 10 g between two syringes with a volume ratio of 2:1. The amounts of catalyst and activator were calculated for the polymerisation of 30 g of monomer; therefore 0.858 mL of EtMgBr was mixed into the syringe containing 20 g of melted monomer and 0.576 mL of NACL was mixed into the syringe containing 10 g of melted monomer. The contents of both syringes were simultaneously injected at 100 mL/min into the dog-bone cavity mould using a Harvard PhD 4400 syringe pump modified to run both syringes parallelly. The preheated syringes were maintained at 150 °C with the help of a heating jacket throughout the injection process.

3. Results and Discussion

3.1. DSC Study

Further, DSC analysis was performed to investigate the thermodynamic properties of the synthesised PMC; in particular, the glass transition temperature, melt onset temperature, melt peak temperature and calculation of the degree of crystallinity.

The DSC results were plotted for all samples with variations in the concentrations of EtMgBr, NACL and EtMgBr + NACL (for each % variation, at least three runs were considered), and are shown in Figure 3a–c.

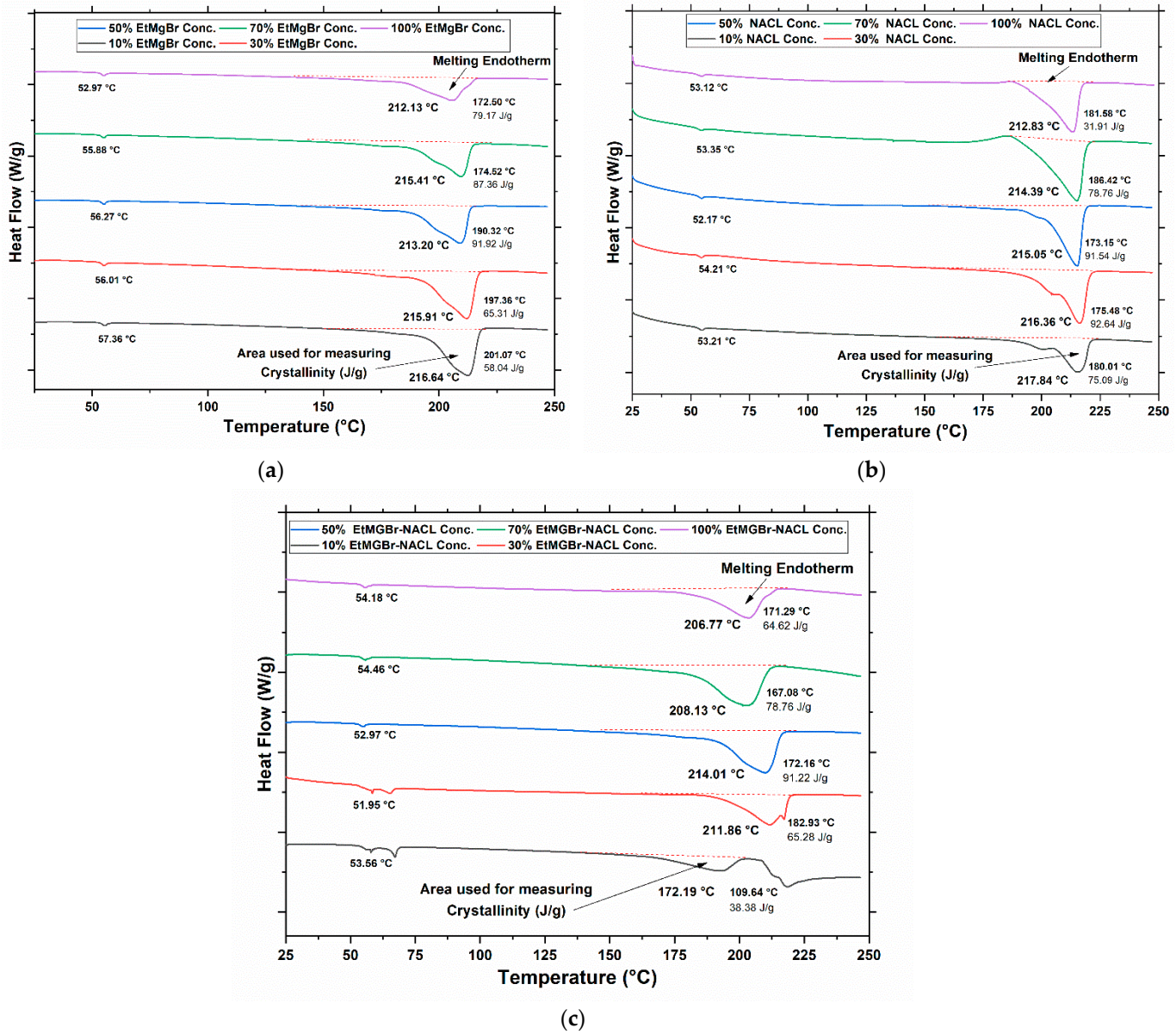

Figure 3. DSC plots for (**a**) the samples with variable concentrations of catalyst (EtMgBr), (**b**) the samples with variable concentrations of activator (NACL) and (**c**) the samples with variable concentrations of both catalyst (EtMgBr) and activator (NACL).

The degree of crystallinity was calculated using the standard formula. The heat of fusion was taken from the DSC plot using the software's functionality, and the area used is shown in Figure 3a–c. The endothermic heat was calculated using this melting peak and using the standard reference value of the heat of fusion for 100% crystalline PA6 as 230 J/g [19]; the calculated crystallinity values for all the samples are summarised in Supplementary Data Section S1.

At the glass transition temperature (T_g), the mechanical properties transition from elastic to brittle due to variations in chain mobility. The transition occurs over a range of temperatures, rather than at a particular fixed temperature and, therefore, the average temperature during this transition is taken as the T_g. The endothermic peak temperature (T_m) is considered the melt temperature. These properties give the detailed characterisation of the formed crystalline phases and their transitions in the synthesised PMC samples and allude to the suitability of the PMC that can suit structural applications.

As seen in Tables S1–S3 in Section S1 of the Supplementary Information, the degree of crystallinity steadily increased with the increase in the EtMgBr concentrations, but dropped after the 50% limit. A similar trend was also seen for the samples with variation in the concentrations of EtMgBr+ NACL. However, when the proportion of the NACL was varied, the samples showed a decreasing trend in the degree of crystallinity once the proportion of NACL was increased above 30%. With the help of DSC plots, it could be deduced that considerable melting and annealing occurred prior to the final melting in all three variations ((EtMgBr, NACL and EtMgBr+ NACL) with proportions equal or higher than 50%. This can be due to the crystal reorganisation and potentially part crystallisation. At more than 50% concentration of EtMgBr, the rapid polymerisation did not provide enough time to rearrange polymer chains into the crystal format [20]. This led to random chain distribution in the solid form, meaning an amorphous phase [20]. As per the results tabulated in Supplementary Information Table S2, the proportion of 30% or 50% NACL should be used as the optimum value to provide the highest degree of crystallinity. However, the higher (>50%) proportion of activator (NACL) increased the polymerisation nucleation sites, resulting in shorter chain formation and potentially resulting in a lower degree of crystallinity [21]. Additionally, at higher concentrations of NACL, EtMgBr or both, the polymerisation reaction was rapid, but non-uniform. This was good for capturing the dispersed state of the nanoparticles, but the polymer chains could not propagate and interlink together due to the presence of unreacted monomers. The somewhat double melting or asymmetric melting endotherms observed for the 10% and 30% NACL variation samples shown in Figure 3b can be possibly explained as the result of either or all of the four contributions from the melting of most original crystals, their recrystallisation, remelting of recrystallised PA6 and melting of residual crystalline regions in the observed samples.

As for the glass transition peak, its associated temperature increased gradually with the increase in the proportion of EtMgBr between 10% and 50%. Although, there is a high possibility that the peak observed at around 50–60 °C can be ascribed to the melting out of the unreacted monomer. Especially, the distinguishingly large peak at 57.36 °C for the 10% sample suggested that most monomers were unreacted in this case, and the melting peak for this sample was comparably small amongst all samples in terms of the endotherm energy released as seen in Figure 3c. Similarly, unreacted monomer was also found in samples with variable proportions of both the catalyst and activator; specifically, the two lowest proportions, i.e., 10–30% of both the catalyst and activator made the polymerisation reaction incapable to complete, resulting in PA6 with the lowest crystallinity; this confirms that the minimum concentration of either catalyst or activator must be at least 50% for successful polymerisation. The lowest-proportion samples (10% and 30%) had mostly unreacted monomers, since the lack of protonating members led to limited polymerising sites. The observations herein suggest that 50% EtMgBr is the optimum concentration for achieving the highest crystallinity in a PMC. The monomer conversion rate for the EtMgBr, NACL and EtMgBr + NACL variation samples was observed to be between 21–100%, 24–100% and 11–100%, respectively.

To confirm the presence of unreacted monomer, a 10% sample was soaked in boiling water to remove unreacted monomers with a melting point of 55 °C. Further, a single ramp-heated DSC study was conducted for this treated sample, yielding the DSC plot included in Figure S1 of the Supplementary Data.

Figure S1 of the Supplementary Data shows the endothermic heat peak around 100 °C, which should be corresponding to the loss of the residual water content left in the samples after boiling them in water before the DSC measurements. The first run gradually started forming the endothermic peak around the water boiling temperature, as it had contained more water. During the second run, the endothermic peak moved to the exact water boiling temperature as the complete loss of the residual water took place at the exact water boiling point. Another endothermic peak corresponding to PMC melting was observed at 215 °C.

However, a smaller peak at 200 °C was observed, which can be assigned to the melting of partially reacted monomer.

The results of the DSC study indicate that both the activator and catalyst, if used at the 50% proportion value, gave the highest degree of crystallinity. Otherwise, the resulting samples lacked the required mechanical properties (degree of crystallinity) desirable for composite sample preparations. Excess of this proportion led to non-uniform polymerisation, wastage of activator, and an even lower degree of crystallinity.

3.2. Thermogravimetric Analysis (TGA) Study

Further study of the thermal degradation of the samples over a range of 100 °C to 800 °C was performed using the thermogravimetric analysis (TGA). After setting the maximum temperature to 800 °C, the standard heat cycle was run for all samples (with all variations concentrations) to study the degradation temperatures of various phases (Figure 4a–c), such as water, monomer, partially polymerised or amorphous phases present in the synthesised PMCs.

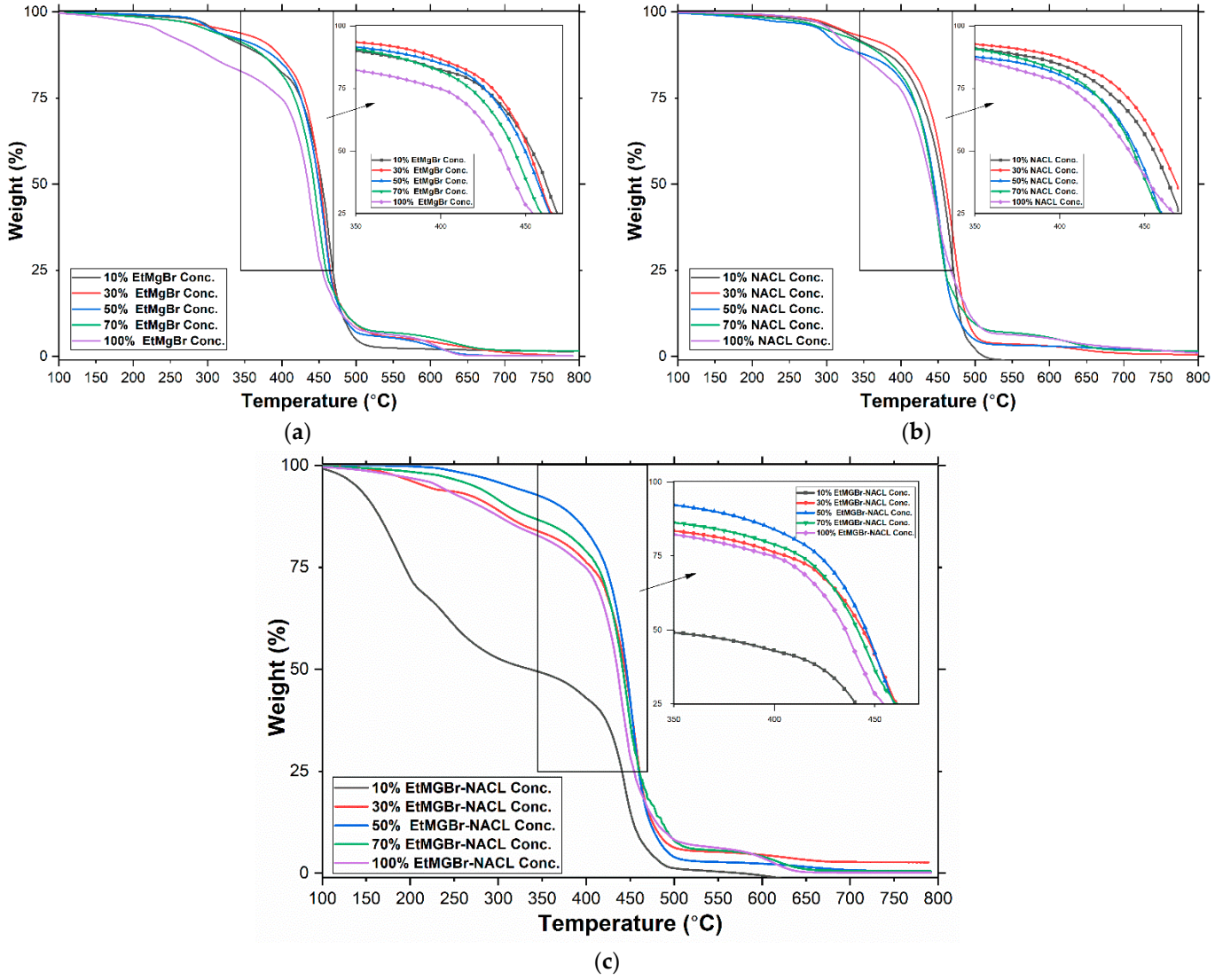

Figure 4. TGA plots depicting weight loss for (**a**) the samples with variable concentrations of catalyst (EtMgBr), (**b**) the samples with variable concentrations of activator (NACL) and (**c**) the samples with variable concentrations of both the catalyst (EtMgBr) and activator (NACL).

For all of the samples, the total mass loss of 99% was observed at the max temperature, and the residue of nanoparticles with approximately 0.15% inert components did not melt at 800 °C. Though, as per the literature values, the thermal degradation of nylon started around 480 °C [22], the synthesised samples with the lower percentage of EtMgBr, as shown in Figure 4a, started degrading at a temperature lower than 480 °C, possibly due to the agglomeration of MNPs. Since PA6 is hygroscopic, the plot shows the weight loss at approximately 150–160 °C, which could be due to the presence of the monomer content and as well as the absorbed moisture. The weight loss varied widely between 1.5–35% and the high weight loss in some cases suggests the only possibility of excess monomer presence.

The samples with different proportions of activator (NACL) showed similar degradation to the standard polyamide samples and are shown in Figure 4b. However, the PMC with lower (10–30%) NACL concentrations showed high degradation. In the range of 350 to 500 °C, the degradation of PMC containing various proportions of EtMgBr was found to be different to that of PMC with various amounts of NACL. NACL of 100% showed the highest gradient of degradation between 180 and 375 °C due to the high amorphous phase content. The highest thermal resistance was illustrated by the 30% NACL proportion sample as compared to all other samples; overall, it performed better against thermal degradation.

The thermogravimetric analysis (TGA) results (Figure 4c) for the PMC with varied EtMgBr + NACL were somewhat similar to those of a standard PA6 sample. Unlike both previous cases, the degradation started from around 150–160 °C and major changes were observed in the 200 to 300 °C region, except for the 10% EtMgBr–NACL sample, which showed drastic degradation in sample weight. The lower, but significant, weight degradation due to temperature was seen for the 30% and 100% samples as well. The TGA result confirms that the higher unreacted monomer content in these samples was unsuitable for any mechanical application. Considering all samples, the superior performance against thermal degradation was shown by the 50% EtMgBr–NACL proportion sample.

3.3. Fourier Transform Infrared Spectroscopy (FTIR) Study

The characterisation of the successfully synthesized PA6-PMC samples with varying concentrations was assessed by analysing their FTIR spectra, as shown in Figure 5a–c. The strong IR bands of commercial PA6 [23] at 3300 cm^{-1}, 1640 cm^{-1} and 1545 cm^{-1}, conforming to the hydrogen-inclusive N–H stretching, the characteristic trans-planar match for amide chain of C=O stretching with amide-I and C–N stretching with the CONH bend of amide-II correspondingly were seen to be shifted slightly to 3293 cm^{-1}, 1633 cm^{-1}, and 1538 cm^{-1}, respectively [20]. This was partly due to the unreacted monomer, and otherwise due to the inclusion of 1 wt% MNPs. Of the amide I and II and N–H stretching bands, the amide II band was especially sensitive to crystalline structure and hence appeared to be shifted with the nano-inclusions (MNPs) and was observed around 1539–1537 cm^{-1} (α-phase). The IR bands for the out–of–plane bends of the N–H (amide V) and C=O (amide VI) groups ideally appeared as relatively sharp bands at 690 cm^{-1} and 580 cm^{-1} for the α-phase, but, due to the MNP inclusions, they shifted to around 685 cm^{-1} and 575 cm^{-1} respectively. Samples with 10%, 30%, and 100% EtMgBr concentrations were observed to have far wider bands close to the individual frequencies associated with the amide group, indicating that the amorphous phase consisted of a wider distribution of α-like and γ-like structures. This, in turn, suggested that they have higher amorphous phase contents (unlike the monomer), which are undesirable for the characteristic mechanical properties built-up for the concerned composite applications in this study.

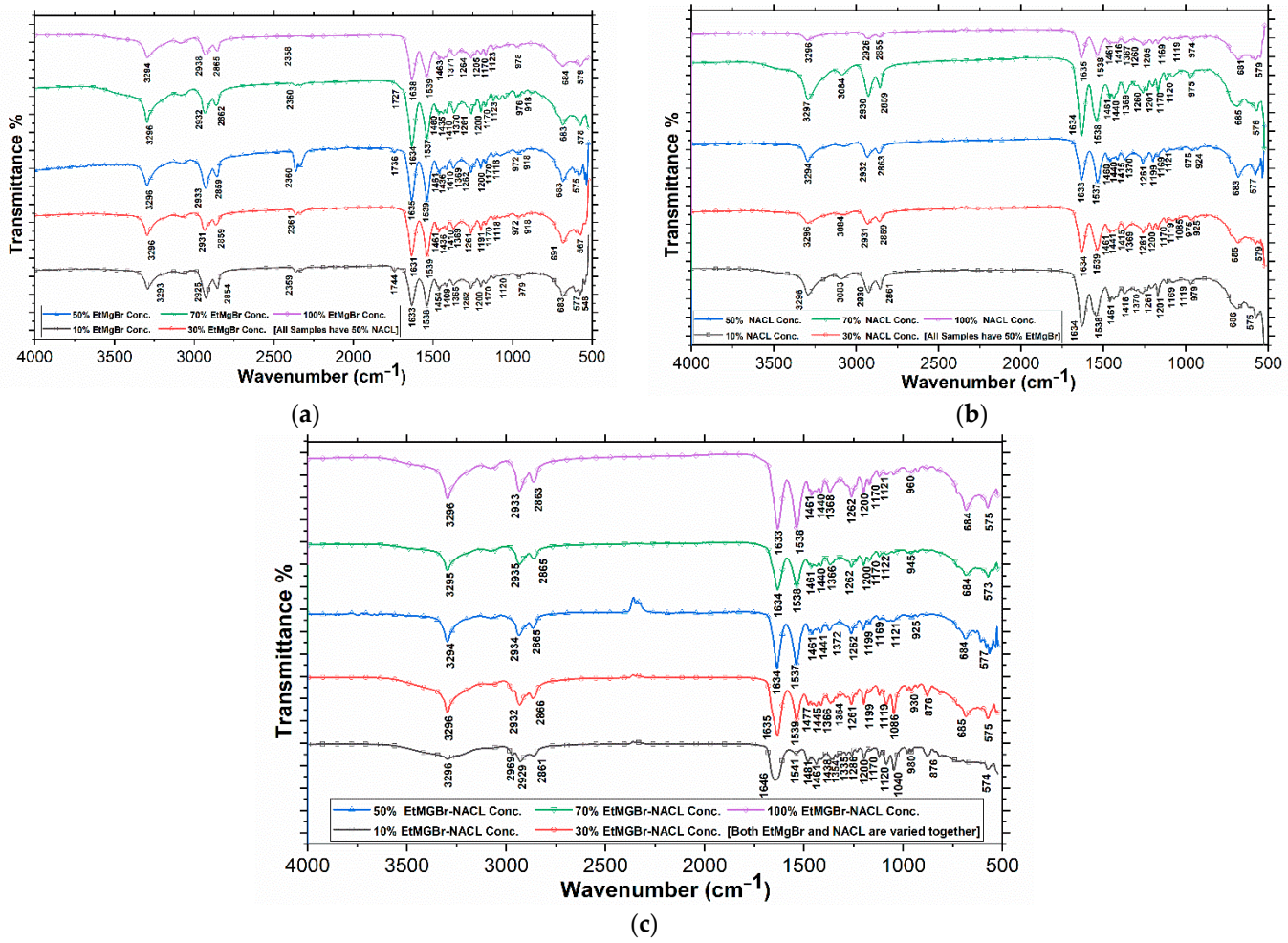

Figure 5. FTIR plots for (**a**) the samples with variable concentrations of catalyst (EtMgBr), (**b**) the samples with variable concentrations of activator (NACL) and (**c**) the samples with variable concentrations of both catalyst (EtMgBr) and activator (NACL).

The strong IR bands for the CH_2 bands adjoining the NH bend and CO bend in the α-phase were herein identified at 1461 cm^{-1} and 1410 cm^{-1}, respectively, instead of their regular occurrences at 1475 cm^{-1} and 1415 cm^{-1}, respectively. The amorphous and γ-phases were both represented by bands at 1460 cm^{-1} (for some samples, at 1461 cm^{-1}) and 1440 cm^{-1} (for some samples, around 1436–1435 cm^{-1}), respectively, and the former was generally observed as a sharp peak in the γ-phase. The two peaks between 1200 cm^{-1} (one of the samples has its appearance at 1205 cm^{-1}) and 1170 cm^{-1} were specifically indicative in all samples. The higher band (1200 cm^{-1} to 1190 cm^{-1}) appeared only in the α-phase, while the lower band (1189 cm^{-1} to 1170 cm^{-1}) indicated amorphous components. The wide band at 1120 cm^{-1} (appearing at 1123 cm^{-1} and 1118 cm^{-1} in most of the samples) was also helpful in examining the amorphous proportion; however, the change to sharp peaks at this band in the 50%, 70% and 100% EtMgBr samples revealed that they had more crystalline contents. The sharp bands observed in the synthesised samples between 980 cm^{-1} (appearing at 979, 978, 976 or 972 cm^{-1} for the prepared samples) and 920 cm^{-1} (appearing at 918 cm^{-1} only for the 30%, 50% and 70% EtMgBr proportion samples) can identify the α- and γ-crystalline phases, respectively [24], further indicating that the 30%, 50% and 70% EtMgBr proportion samples had higher crystalline contents. The peak near 686 cm^{-1} corresponded to the Fe-O bond stretching of iron oxide [25], confirming the presence of MNPs, and even related to the amide V (α and β) content of the pristine PA6.

Generally, the IR spectrum of PA6 shows the amide I stretching as normally an intense peak, and its regular occurrence is observed around 1640 cm^{-1}. This presence is correspond-

ing to the C=O double bond stretching mode and was observed around 1638–1631 cm^{-1} for all of the prepared EtMgBr varying-proportion samples. The disorder is observed herein with the varying concentrations of EtMgBr in samples that had unreacted monomer either due to insufficient EtMgBr (10% EtMgBr proportion sample) or with high contents of EtMgBr (70% and 100% EtMgBr proportion samples) that created very rapid polymerisation of the monomer + EtMgBr solution that came in immediate contact with the activator (NACL). This was concluded based on the comparison of the amide I and the amide II stretching extents—the higher amide I stretch represents more disorder [26] in the 10%, 70% and 100% EtMgBr samples.

The FTIR spectra in Figure 5b show the successful synthesis of PA6-PMC samples with different NACL proportions. The samples with 10% and 100% NACL proportions were observed to have much wider bands close to every frequency related to the amide group and showed that the amorphous phase consisted of broader distributions of α-like and γ-like structures. This shows that they had high amorphous phase proportions, which is undesirable for general mechanical and thermodynamic properties.

Similar to the EtMgBr FTIR results, the peaks at 1461 cm^{-1} (for the 50% NACL proportion sample it appeared at 1460 cm^{-1}) and 1440 cm^{-1} (for the 30% NACL proportion sample, it appeared at 1441, and for the 50% and 70% NACL proportion samples, it appeared at 1440 cm^{-1}) corresponded to amorphous and γ-phases. The 10% and 100% NACL proportion samples did not show the 1440 cm^{-1} peak, indicating their lower crystalline content. The two peaks between 1200 cm^{-1} (the samples had its appearance around 1205–1199 cm^{-1}) and 1170 cm^{-1} (some samples showed its presence at 1169 cm^{-1}) were present in all samples, though the 1170 peak representing α-phase was quite sharp in only the 30%, 50% and 70% NACL proportion samples, which demonstrates the higher crystalline content. The wide band at 1120 cm^{-1} (appearing around 1121 cm^{-1} and 1119 cm^{-1} in most of the samples) was also helpful for examining the amorphous concentrations. The sharp bands observed in the synthesised samples between 980 cm^{-1} (appearing around 979, 975 or 974 cm^{-1} for the prepared samples) and 920 cm^{-1} (appearing at 925 cm^{-1} and 924 cm^{-1} only for the 30% and 50% NACL proportion samples) were similar to previous samples, referring to the α- and γ- crystalline phases, respectively [24].

The amide I band appearing at 1640 cm^{-1} highlighted the polyamide backbone. The stretching mode of the C=O double bond also appeared around 1635–1633 cm^{-1} for all of the prepared NACL samples, which was similar to PA6. The disappearance of the peak at 3084 cm^{-1} for the 50% EtMgBr, 100% EtMgBr and 10% EtMgBr + NACL samples was seen to be related to the reduced stretching of bonds in the absence of long polymer chains. The NACL provided more chain initiation sites, leading to rapid chain formation, but of short length. The sample with the 100% NACL proportion also had a noteworthy concentration of NACL remaining unreacted, because of unbalanced mixtures resulting from the rapid polymerisation of the top surface monomer + EtMgBr solutions.

The characterisation of the successful synthesis of the PA6-PMC samples was assessed by FTIR, and their spectra are shown in Figure 5c; most IR bands in the PMC samples with varying EtMgBr and NACL concentrations were found to be the same as those observed in PA6 PMCs produced by varying the catalyst or activator individually. Samples with 10%, 30% and 100% EtMgBr and NACL concentrations were observed with much broader bands associated with the amide group compared to PMC the samples produced by varying the catalyst and activator separately, indicating that the amorphous phase consisted of a wider distribution of the α-like and γ-like structures. The spectrum of 10% EtMgBr + NACL showed no or a very small amount of polymerisation.

Most peaks in the signature section of all spectra were found to be similar to those of the other samples described in the previous two sections. However, the bond formation was significantly affected by the variation in the EtMgBr + NACL concentration, as observed in the large modification of the peak located in the bonding region of the FTIR plots. The wide band at 1120 cm^{-1} (also appearing at 1121 cm^{-1} and 1119 cm^{-1}) appeared only for the 50%, 70% and 100% EtMgBr and NACL proportion samples and suggests their

amorphous phase contents. However, the change to sharp peaks at this band in the 10% and 30% EtMgBr and NACL proportion samples revealed the significant bond formation in absence of lower bond formation in the range of 2660–3300 cm^{-1}. Here, the peak near 685–684 cm^{-1} also corresponds to the Fe-O bond stretching and amide V (α and β) content of the pristine PA6 [25].

The 1640 cm^{-1} amide I band corresponding to the C=O double bond stretching mode was observed around 1646–1633 cm^{-1} for the prepared samples. Observing the shifts in the amide I and amide II bands, disorder was observed [26] herein with the varying concentrations of EtMgBr and NACL proportions in samples that had either unreacted monomers due to insufficient EtMgBr and NACL (10% EtMgBr and NACL proportion sample) or high contents of EtMgBr and NACL proportion (70% and 100% EtMgBr and NACL proportion samples) that created very rapid polymerisation of the monomer + EtMgBr solution after contacting the activator (NACL). In this case, the excess/unreacted NACL was left above the prepared sample surface due to insufficient mixing arising from the very quick polymerisation reaction.

3.4. X-ray Diffraction Study

The X-ray diffraction (XRD) results in Figure 6a–c show two reflection peaks at Bragg angles of 24° 2θ (3.7 Å) and 21° 2θ (4.2 Å), related to the reflections of the crystalline planes (002)/(202) and (200) respectively, referring to monoclinic α-phase with higher tensile strength [27,28]. The reflection peak at a diffraction angle of 21°, which corresponded to the γ-form of PA6, started appearing in the samples containing an EtMgBr concentration (Figure 6a) higher than 50%, pointing towards the loss of tensile strength. The even broadening of both peaks related to the α-phase suggested the amorphous phase. In the 100% EtMgBr sample, other peaks appeared, showing additional phases with lower Bragg angles. The minor peaks observed at 17° 2θ, 22° 2θ and 28° 2θ can be identified as the γ-phase of PA6 with corresponding miller indices of (020), (001) and (200)/(201) [29]. The achieved crystallite sizes for all the EtMgBr variation samples are included in Table S4 in Section S3 of the Supplementary Data.

The overall characterisation trend clearly implies that the polymerisation happened very quick as the proportion of nucleophilic EtMgBr increased. However, there were some volumes of it remaining unreacted in the polymerisation, hence indicating that it was not desirable to have a higher proportion of EtMgBr for polymerisation beyond the quantified measures noted.

As seen in Figure 6b, the multiple reflection peaks at various Bragg angles in the 10% sample showed the presence of multiphase transitions. Further, the trend of the broadening of the reflection peaks related to two α-phase peaks with an increase in the content of NACL was visible; however, the broadening was not high, as seen in the samples containing variable EtMgBr concentrations. The emergence of the γ- phase-related reflection peak around a Bragg angle of 21° was very small compared to those of the EtMgBr samples. The achieved crystallite sizes for all the NACL variation samples are included in Table S4 in Section S3 of the Supplementary Data. The overall results suggest that, with the increase in NACL concentration in PA6, the loss of tensile strength related to α-phase was not as high as that in the sample with increased EtMgBr concentrations. The EtMgBr concentration increase was responsible for the high polymerisation rate and reducing time to allow effective molecular chain rearrangement; however, the NACL concentration increase provided more nucleating sites for polymerisation to take place, forming shorter chains [30]; however, it does did reduce the time for polymerisation, resulting in a thermally more stable α-phase.

As seen in Figure 6c, the PA6 characteristic XRD reflection peaks at two Bragg angles displayed the multiphase formation for the samples with 10% and 30% EtMgBr and NACL proportions. The reflection peaks for the 10% and 30% concentration samples even showed incomplete polymerisation.

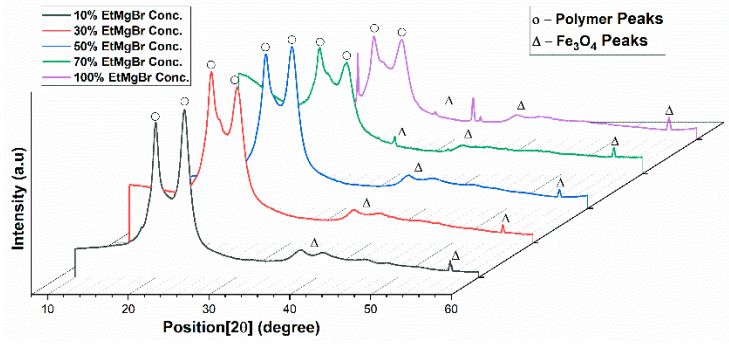

(**a**)

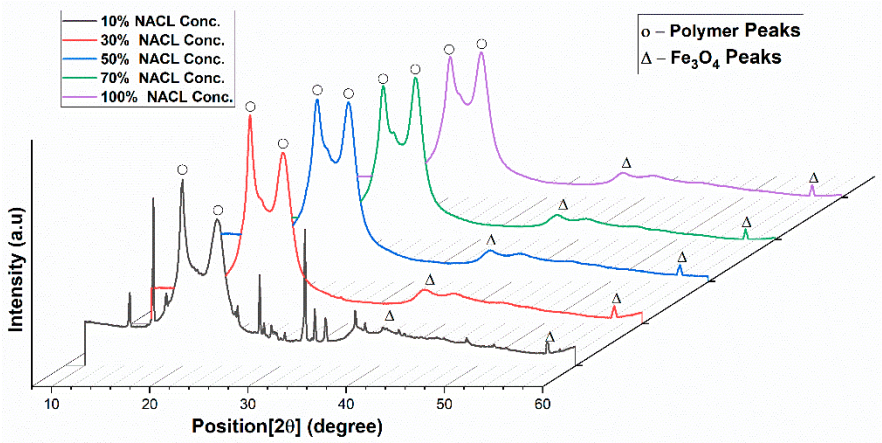

(**b**)

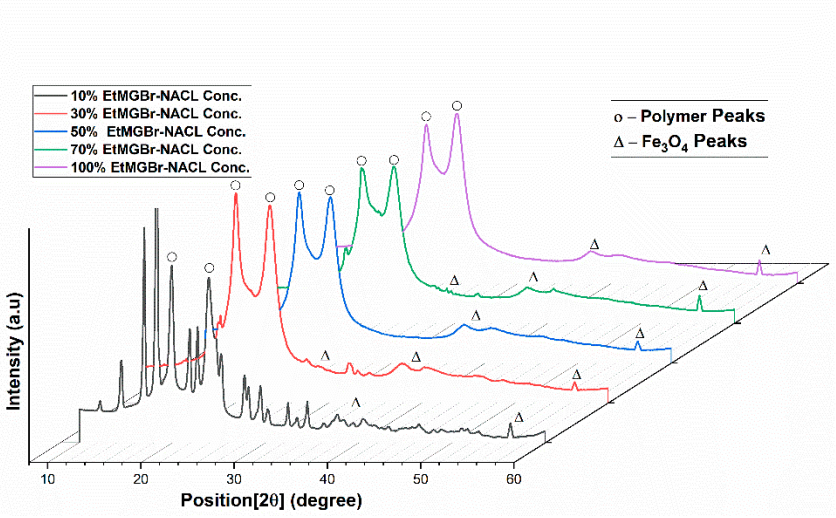

(**c**)

Figure 6. (**a**) XRD plots for (**a**) the samples with variable concentrations of catalyst (EtMgBr), (**b**) the samples with variable concentrations of activator (NACL) and (**c**) the samples with variable concentrations of both catalyst (EtMgBr) and activator (NACL).

The samples with 70% and 100% concentrations did not show strong reflection peaks related to the γ-phase; however, the broader peaks compared to those of the 50% sample confirmed the presence of a significantly larger percentage of the amorphous phase, leading to mechanically weaker phase formation. The achieved crystallite sizes for all of the EtMgBr + NACL variation samples are included in Table S4 in Section S3 of the Supplementary Data. Overall, the comparison of all the samples here showed that, except

for the 50% EtMgBr + NACL sample, all other samples were unsuitable due to either their incomplete formation or higher amorphous tendency.

3.5. Selection of Optimum Proportion

Based on the FTIR study from the proportion variations of EtMgBr, NACL and EtMgBr + NACL, it was observed that most of the samples (except for the 10% EtMgBr + NACL proportion sample) were mostly following the PA6 backbone, although with varying amorphous/crystalline contents, confirming that most of them were synthesised almost to the level of commercial PA6 PMC. The thermal degradation study also showed similar responses from all of the samples (except the complete distinguishing and degraded performance by the 10% EtMgBr + NACL proportion sample). Therefore, the main criteria of comparison can be taken as that of the highest degree of crystallinity level achieved by any individual sample, as indicated by the DSC results. This criterion would also ensure that the best candidate is selected, fulfilling the better mechanical property of film formability, crucial for the composite film preparation to prepare the composite samples. Figure 7a,b compares the degree of crystallinity and γ-phase achieved by the samples with varying concentrations of EtMgBr, NACL and EtMgBr + NACL.

The comparison plot clarifies that the samples with the 50% EtMgBr proportion, or, in other words, with 50% NACL proportion (also termed as 50% EtMgBr + 50% NACL) had similar degrees of crystallinity (%), which is obvious as they were all practically the same samples, just prepared in slightly different manners. Moreover, the γ-phase was least present in the sample with 50% EtMgBr + 50% NACL, which is desirable for high tensile strength and a stable phase. Nevertheless, the highest degree of crystallinity (%) was noted for the sample with a 30% NACL proportion (50% EtMgBr proportion) amongst all the samples, and it was almost comparable to that which was observed in the 50% NACL proportion (50% EtMgBr proportion) sample mentioned before. So, as a matter of choice, either one could be selected as the optimum proportion for giving the highest degree of crystallinity (%) and presence of a large amount of the α-phase (mechanically high tensile strength) or absence of the γ-phase (Figure 7b, less preferable for toughness). However, to ensure the efficient utilisation of resources, the 50% NACL proportion (with 50% EtMgBr proportion) should be selected as the optimum proportion; this would ensure that no excess/unreacted NACL is left during the polymerisation process.

3.6. Composite Part Rapid Prototyping

This unique application involves utilising the melted monomer and MNP mixture to be injected in the designed mould to form a composite dog-bone sample part, the concept being that of the plastic injection moulding would facilitate rapid prototyping of composite PMC dog-bone parts for multifunctional applications, such as self-healing components. The choice of dog-bone sample preparation was just a matter of choice for the illustration purpose, but the proposed setup can be used for the prototyping of any shape of sample, as long as the compatible mould can be feasibly built. Since the melt monomer and MNPs mixture were directly introduced into the glass syringes, it was first challenging to maintain the melt state. However, with an additionally designed uniform heating jacket setup for the syringes, this issue was later overcome. There was also a possibility of uneven mixing due to the challenge in pumping the mixtures together, due to the Y channel becoming partially blocked. As the resulting mixture was observed to be rapidly polymerising when introduced to the dog-bone mould, this could also be the main reason for the partial blockage of the Y channel. The composite sample formed is shown in Figure 8.

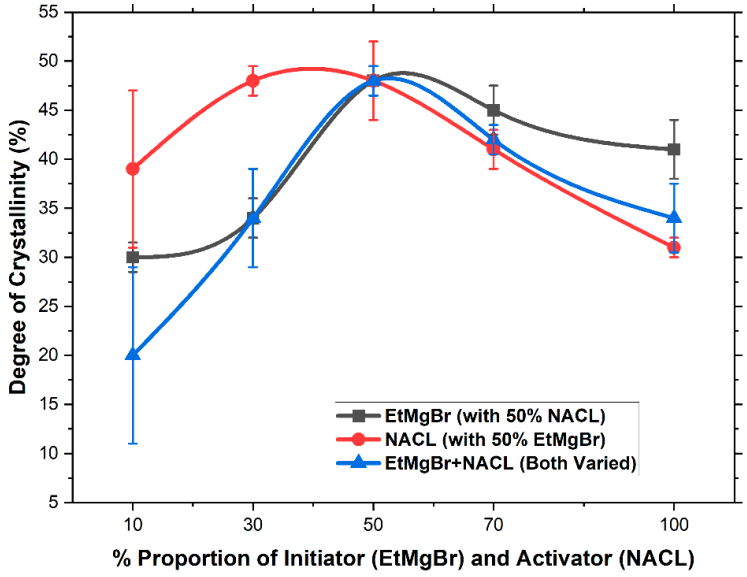

(**a**)

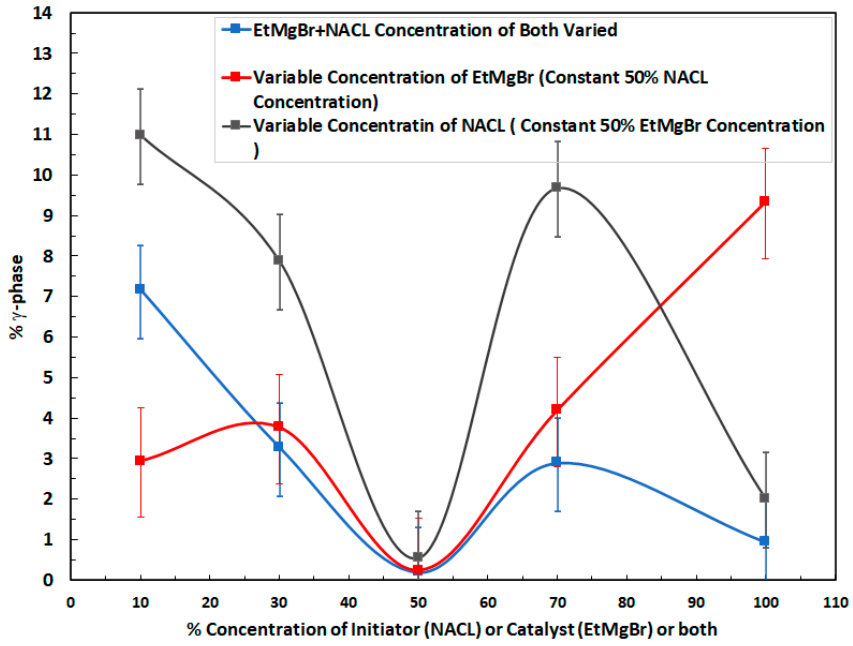

(**b**)

Figure 7. (**a**) Comparison between the degree of crystallinity of each sample with varying concentrations of EtMgBr, NACL and EtMgBr + NACL. (**b**) Comparison of % γ-phase in each sample with variations in the concentrations of EtMgBr, NACL and EtMgBr + NACL. In both plots, each data point on EtMgBr + NACL line (blue) represents the same % concentration of activator and catalyst as shown on the *X*-axis, whereas the EtMgBr and NACL lines (grey and red, respectively) represent variable % of EtMgBr (corresponding to those shown on the *X*-axis) concentrations at a 50% NACL proportion and variable % concentrations (corresponding to those shown on the *X*-axis) of NACL at a 50% concentration of EtMgBr.

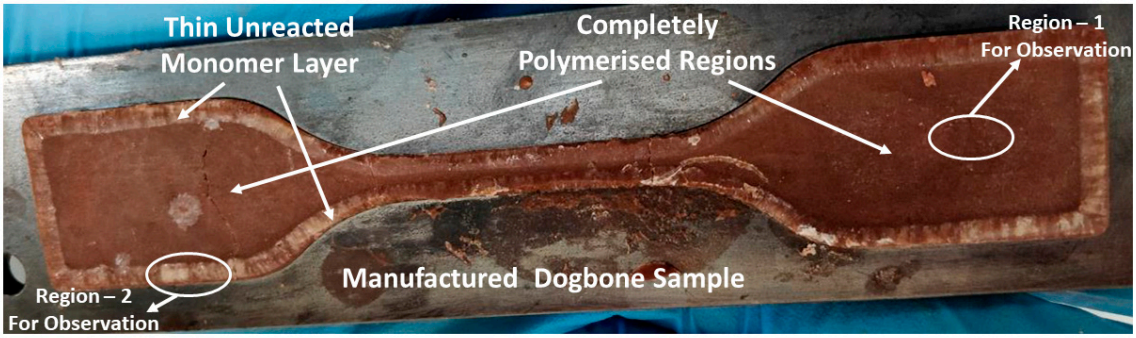

Figure 8. The synthesised multifunctional PMC dog-bone sample with the designed rapid prototyping setup.

Though most of the resulting dog-bone sample region was polymerised, there were visible traces of unreacted monomer towards the edges, as highlighted in Figure 8. The temperature of the monomer at the edge of the room-temperature steel mould possibly dropped below the minimum temperature required for the polymerisation and remained unreacted. A possible future fix for this could be adding another setup for preheating the mould before the mixture's injection. The characterisation of the prepared dog-bone sample revealed that approximately 30% of the sample volume was unreacted monomer and the reason for this can be attributed to the possible uneven mixing during the injection process through the Y connector region. To quantify the quality of the polymerised (marked as Region 1) and partly polymerised (marked as Region 2) regions of the sample, DSC analysis was conducted. The DSC analysis results of two distinctive regions (marked as Regions 1 and 2 in Figure 8) are summarised in Table S5 of Section S4—Supplementary Data, with degrees of crystallinity of 44.29% and 40.16% attained in analysed regions 1 and 2, respectively. The composite sample showed a 60–85% monomer conversion rate, as measured using the DSC method. Even though partially formed, the completely polymerised regions showed their degree of crystallinity, crystallite size, and phase to be the same as those of the tested PA6 PMC, confirming the successful creation and usage of the prototyped part.

4. Conclusions

Manufacturing multifunctional PMCs parts with adequate mechanical properties and additional functionality (self-healing) at a large scale requires control over its degree of crystallinity and crystallite type. In this work, it was demonstrated that the nanoparticle-influenced crystallisation process during the anionic polymerisation of PA6 PMC can be altered favourably by using a suitable combination of catalyst and activator. However, the DSC, TGA, FTIR, and XRD characterisation results of samples with variations of EtMgBr, NACL, and EtMgBr + NACL indicated that neither the proportion of catalyst or activator should be too high or too low for the polymerisation process. As an overall comparison, it was found that the combination of 30% activator (NACL) and 50% catalyst (EtMgBr) proportion was most favourable in achieving the highest degree of crystallinity and small crystallites containing mostly α-phase in a magnetic PMC with 1 wt% iron oxide nanoparticles, which is most desirable for the tensile strength and inducing magnetoelectric effect as a multifunctional component. Further, as an example, the rapid prototyping of a PMC dog-bone sample with the optimised concentrations of catalyst and activator was demonstrated to present its use case for the large-scale manufacturing of multifunctional polymer PMC components.

Supplementary Materials: The following supporting information can be downloaded at: https://www.mdpi.com/article/10.3390/jcs6030083/s1.

Author Contributions: Conceptualization, R.G. and K.P.; methodology, R.G.; formal analysis, R.G.; investigation, R.G.; resources, R.G., K.P. and J.N.; data curation, R.G.; writing—original draft preparation, R.G.; writing—review and editing, R.G. and K.P.; visualization, R.G.; supervision, K.P.; project

administration, R.G. and K.P.; funding acquisition, K.P. and J.N. All authors have read and agreed to the published version of the manuscript.

Funding: This research was funded by the Robert Gordon University.

Data Availability Statement: The related data as discussed in this article can be requested from the corresponding author (R.G.).

Acknowledgments: The authors are grateful to the School of Pharmacy at Robert Gordon University for making their facility available for part of this research.

Conflicts of Interest: The authors declare no conflict of interest.

References

1. Gojny, F.H.; Nastalczyk, J.; Roslaniec, Z.; Schulte, K. Surface modified multi-walled carbon nanotubes in CNT/epoxy-composites. *Chem. Phys. Lett.* **2003**, *370*, 820–824. [CrossRef]
2. Ali, A.; Andriyana, A. Properties of multifunctional composite materials based on nanomaterials: A review. *RSC Adv.* **2020**, *10*, 16390–16403. [CrossRef]
3. Gupta, R.; Huo, D.; White, M.; Jha, V.; Stenning, G.B.; Pancholi, K. Novel Method of Healing the Fibre Reinforced Thermoplastic Composite: A Potential Model for Offshore Applications. *Compos. Commun.* **2019**, *16*, 67–78. [CrossRef]
4. Gupta, R.; Pancholi, K.; De, S.; Rulston Murray, D.; Huo, D.; Droubi, G.; White, M.; Njuguna, J. Effect of Oleic Acid functionalised Iron Oxide Nanoparticles on Properties of Magnetic Polyamide-6 Nanocomposite. *J. Miner. Met. Mater. Soc. (TMS)* **2019**, *71*, 3119–3128. [CrossRef]
5. Gupta, R.; Staknevicius, R.; Pancholi, K. Rapid Multifunctional Composite Part Manufacturing using Controlled In-situ Polymerization of PA6 Nanocomposite. *Procedia CIRP* **2019**, *85*, 61–65. [CrossRef]
6. Gupta, R.; Pancholi, K.; Prabhu, R.; Pancholi, M.; Huo, D.; Jha, V.; Latto, J. Integrated self-healing of the composite offshore structures. In *OCEANS 2017-Aberdeen*; IEEE: Aberdeen, UK, 2017.
7. Gupta, R.; Smith, L.; Njuguna, J.; Deighton, A.; Pancholi, K. Insulating MgO-Al_2O_3-LDPE Nanocomposites for Offshore Medium Voltage DC Cable. *ACS Appl. Electron. Mater.* **2020**, *2*, 1880–1891. [CrossRef]
8. Gupta, R.; Badel, B.; Gupta, P.; Bucknall, D.G.; Flynn, D.; Pancholi, K. Flexible Low-Density Polyethylene–$BaTiO_3$ Nanoparticle Composites for Monitoring Leakage Current in High-Tension Equipment. *ACS Appl. Nano Mater.* **2021**, *4*, 2413–2422. [CrossRef]
9. Zhang, X.; Fan, X.; Li, H.; Yan, C. Facile preparation route for graphene oxide reinforced polyamide 6 composites via in situ anionic ring-opening polymerization. *J. Mater. Chem.* **2012**, *22*, 24081–24091. [CrossRef]
10. Liu, L.; Wagner, H.D. Rubbery and glassy epoxy resins reinforced with carbon nanotubes. *Compos. Sci. Technol.* **2005**, *65*, 1861–1868. [CrossRef]
11. Velasco-Santos, C.; Martínez-Hernández, A.L.; Fisher, F.T.; Ruoff, R.; Castaño, V.M. Improvement of thermal and mechanical properties of carbon nanotube composites through chemical functionalization. *Chem. Mater.* **2003**, *15*, 4470–4475. [CrossRef]
12. Paiva, M.; Zhou, B.; Fernando, K.; Lin, Y.; Kennedy, J.; Sun, Y. Mechanical and morphological characterization of polymer–carbon nanocomposites from functionalized carbon nanotubes. *Carbon* **2004**, *42*, 2849–2854. [CrossRef]
13. Goff, J.; Whelan, T.; DeLaney, D. The Dynisco extrusion processors handbook. *Edition* **2000**, *2*, 284.
14. Peng, X.; Zhang, M.; Guo, Z.; Sang, L.; Hou, W. Investigation of processing parameters on tensile performance for FDM-printed carbon fiber reinforced polyamide 6 composites. *Compos. Commun.* **2020**, *22*, 100478. [CrossRef]
15. Coleman, J.N.; Khan, U.; Gun'ko, Y.K. Mechanical reinforcement of polymers using carbon nanotubes. *Adv Mater.* **2006**, *18*, 689–706. [CrossRef]
16. Balazs, A.C.; Emrick, T.; Russell, T.P. Nanoparticle polymer composites: Where two small worlds meet. *Science* **2006**, *314*, 1107–1110. [CrossRef]
17. Ito, H.; Russell, T.P.; Wignall, G. Interactions in mixtures of poly (ethylene oxide) and poly (methyl methacrylate). *Macromolecules* **1987**, *20*, 2213–2220. [CrossRef]
18. Vicard, C.; De Almeida, O.; Cantarel, A.; Bernhart, G. Experimental study of polymerization and crystallization kinetics of polyamide 6 obtained by anionic ring opening polymerization of ε-caprolactam. *Polymer* **2017**, *132*, 88–97. [CrossRef]
19. Blaine, R.L. *Determination of Polymer Crystallinity by DSC*; TA Instruments: Newcastle, Germany, 2013.
20. Tung, J.F. Synthesis and Characterisation of Polyamide 6 Blends Made by Reactive Extrusion. Ph.D. Thesis, Brunel University School of Engineering and Design, Uxbridge, UK, 1993.
21. Ageyeva, T.; Sibikin, I.; Karger-Kocsis, J. Polymers and related composites via anionic ring-opening polymerization of lactams: Recent developments and future trends. *Polymers* **2018**, *10*, 357. [CrossRef]
22. Braun, E.; Levin, B.C. Nylons: A review of the literature on products of combustion and toxicity. *Fire Mater.* **1987**, *11*, 71–88. [CrossRef]
23. Arimoto, H. α–γ Transition of nylon 6. *J. Polym. Sci. Part A Gen. Pap.* **1964**, *2*, 2283–2295. [CrossRef]
24. Mottus, E.H.; Hedrick, R.M.; Butler, J.M. Preparation of Polycaprolactam Using N-Acyl Activators. U.S. Patent 3,017,391, 16 January 1962.

25. Navale, S.; Khuspe, G.; Chougule, M.; Patil, V. Camphor sulfonic acid doped PPy/α-Fe_2O_3 hybrid nanocomposites as NO_2 sensors. *RSC Adv.* **2014**, *4*, 27998–28004. [CrossRef]
26. Šebenda, J.; Kraliček, J. Effect of imides on the alkaline polymerisation of caprolactam. *Collect. Czech. Chem. Commun.* **1958**, *23*, 766–767. [CrossRef]
27. Khanna, Y.P.; Chomyn, G.; Banerjie, A.; Reimschuessel, A.C. Nucleating System for Polyamides. U.S. Patent 4,749,736, 7 June 1988.
28. Ramírez, L.P.; Landfester, K. Magnetic polystyrene nanoparticles with a high magnetite content obtained by miniemulsion processes. *Macromol. Chem. Phys.* **2003**, *204*, 22–31. [CrossRef]
29. Porter, R. *Macromolecular Physics, Volume 3—Crystal Melting, Bernhard Wunderlich*; Academic Press: New York, NY, USA, 1980; 363p.
30. Rusu, G.; Ueda, K.; Rusu, E.; Rusu, M. Polyamides from lactams by centrifugal molding via anionic ring-opening polymerization. *Polymer* **2001**, *42*, 5669–5678. [CrossRef]